arXiv:cond-mat/9708024v1 4 Aug 1997

Cumulant expansion of the periodic Anderson model in infinite dimension

M. E. Foglio*
Instituto de Fisica "Gleb Wataghin"
Universidade Estadual de Campinas,UNICAMP
13083-970 Campinas, São Paulo, Brasil

M. S. Figueira
Instituto de Fisica, Universidade Federal Fluminense,UFF
24000-970 Niterói, Rio de Janeiro, Brasil
(February 1, 2008)

The diagrammatic cumulant expansion for the periodic Anderson model with infinite Coulomb repulsion ($U = \infty$) is considered here for an hypercubic lattice of infinite dimension ($d = \infty$). The nearest neighbor hopping of the uncorrelated electrons is described exactly by a conduction band, while two different models of hybridization are treated as a perturbation. The same type of simplifications obtained by Metzner for the cumulant expansion of the Hubbard model in the limit of $d = \infty$, are shown to be also valid for the periodic Anderson model. The derivation of these properties had to be modified because of the exact treatment of the conduction band.

71.28.+d, 71.27.+a, 71.10.+x, 75.20.Hr

I. INTRODUCTION

The periodic Anderson model (PAM) gives a schematic description of very important systems with strongly correlated electrons, and there are several recent reviews on this subject[1]. The model consists of a lattice with two localized electronic states at each site, strongly correlated by a Coulomb repulsion U, plus a band of uncorrelated conduction electrons (c-electrons) that hybridize with the localized electrons (f-electrons). The cumulant expansion of the PAM discussed in this work is a perturbative expansion around the atomic limit, and is an extension[2] of the method originally employed by Hubbard[3] to study his well known model of correlated itinerant electrons[4]. He introduced operators $X_{j,ba} =\mid j, b\rangle\langle j, a \mid$, that transform the local state $\mid a\rangle$ at site j into the local state $\mid b\rangle$ at the same site, and developed a diagrammatic method that circumvents the fact that the X operators are neither fermions nor bosons. His work was the first application of the cumulant expansion to a quantum system of fermions[5] and has several desirable properties: it seems to be a natural extension of the usual diagrammatic techniques, it does not have excluded site problems in the lattice summations and it is possible to derive a linked cluster expansion for the grand canonical potential(see ref.[2] for more details). At the same time, the use of X operators allows to work in a subspace of the whole space of local states, that contains only the states that are relevant to the problem of interest. It seems therefore useful to understand better this method, and the main purpose of the present paper is to study the properties of the cumulant expansion for the PAM in the limit of infinite spatial dimensions ($d \to \infty$).

Metzner and Vollhardt[6] have recently applied the limit $d \to \infty$ to strongly correlated fermion systems, providing non-trivial models of the Hubbard type that are substantially simpler to analyze. This development has stimulated many new works, and we could mentioned the very successful Dynamical Mean Field Theory[7], that uses the local properties of the self energy for $d \to \infty$ as a starting point. Several methods have been employed to study the PAM in this limit[8−11], and the cumulant expansion of the Hubbard model was reconsidered by Metzner[12], showing that there is an important reduction in the number and type of cumulant diagrams that appear in the expansion when $d \to \infty$ in an hypercubic lattice. In the Hubbard model there is no hybridization and

---

[*] Associate Member of ICTP,Trieste,Italy

the hopping Hamiltonian is used as perturbation, while the PAM is usually employed to model systems with a bandwidth much larger than the hybridization energies, and it is then preferable to diagonalize the conduction band and use the hybridization Hamiltonian as perturbation. It was then necessary to make substantial modifications to Metzner's derivation in order to apply it to the PAM when $d \to \infty$.

In the following sections two types of hybridization models are considered: the purely "local" hybridization and the "nearest neighbor" (n.n.) one. In the n.n. hybridization there are electronic transitions between localized ("f") states at a site and conduction Wannier states at the nearest neighbor sites, while in the local hybridization those transitions only occur at the same site. The same type of diagram cancellation obtained by Metzner for the Hubbard model is obtained for these two hybridization models in the PAM.

As the local hybridization between f and d or s electrons should vanish when the site has inversion symmetry, the n.n. hybridization discussed in this paper is more realistic than the local one, because it does not necessarily vanish for that type of site. The local approximation is usually employed because it makes the calculation simpler; and the changes introduced by an interatomic hybridization have been already discussed in the case of a diatomic-molecule model[13].

II. THE HYPERCUBIC LATTICE

Let us consider free electrons in an hypercubic lattice of dimension d, described by a Hamiltonian[14]

$$H_c = \sum_{\mathbf{n},\mathbf{m},\sigma} t_{\mathbf{n},\mathbf{m}}\, C^\dagger_{\mathbf{n},\sigma}\, C_{\mathbf{m},\sigma} \tag{2.1}$$

with translational invariance. The position of the site $\mathbf{n} = (n_1, \ldots, n_d)$ is given by $\mathbf{R_n} = \sum_{\alpha=1}^{d} \mathbf{e}_\alpha\, n_\alpha$, where $|\mathbf{e}_\alpha| = a$ is the lattice parameter and the n_j are integers. Only n.n. hopping shall be considered, so that $t_{\mathbf{n},\mathbf{m}}$ is non-zero and equal to $-\bar{t}$ when the components m_α of $\mathbf{m}$ satisfy $m_\alpha = n_\alpha + \delta_{\alpha,\gamma}$ for $\gamma = 1, 2, \ldots, d$. Employing the Wannier transformation

$$C_{\mathbf{n},\sigma} = \frac{1}{\sqrt{N}} \sum_{\mathbf{k},\sigma} C_{\mathbf{k},\sigma}\ \exp[i\mathbf{k}.\mathbf{R_n}] \quad , \tag{2.2}$$

with $\mathbf{k}$ satisfying cyclic boundary conditions, one obtains

$$H_c = \sum_{\mathbf{k},\sigma} E_{\mathbf{k}}\, C^\dagger_{\mathbf{k},\sigma}\, C_{\mathbf{k},\sigma} \quad , \tag{2.3}$$

where

$$E_{\mathbf{k}} = -2\, t \sum_{s=1}^{d} \cos(k_s\ a) \quad . \tag{2.4}$$

The electronic Green's functions (GF) for imaginary time are defined by[2]

$$G_\sigma(\mathbf{k},\tau) \equiv \left\langle \left(C_{\mathbf{k},\sigma}(\tau)\ C^\dagger_{\mathbf{k},\sigma} \right)_+ \right\rangle \quad , \tag{2.5}$$

where $C_{\mathbf{k},\sigma}(\tau) \equiv \exp[H_c\tau]\ C_{\mathbf{k},\sigma}\ \exp[-H_c\tau]$ and the subindex $+$ in Eq.(2.5) is the usual chronological ordering of Fermi operators, with τ increasing to the left. To emphasize that the hybridization was not considered in these GF, they will be denoted with $G^0_\sigma(\mathbf{k},\tau)$, and after Fourier transformation in the imaginary time τ they are given by[15] $G^0_\sigma(\mathbf{k},\omega_\nu) = -(i\omega_\nu - E_{\mathbf{k}})^{-1}$. To obtain a finite average energy per site when $d \to \infty$, it is necessary to renormalize H_c, taking a finite t in the non-zero $t_{\mathbf{n},\mathbf{m}} = -t/\sqrt{2d}$ (i.e. when $\mathbf{n}$ and $\mathbf{m}$ are n.n.). In that limit the energy density of states is given by[14]

$$\rho_d(E) = \frac{1}{\sqrt{2\pi t^2}} \exp\left[-\frac{E^2}{2\ t^2}\right] \quad , \tag{2.6}$$

and

$$\left\langle \left(E(\mathbf{k})\right)^2 \right\rangle = t^2 \quad . \tag{2.7}$$

The exact solution of H_c is used in the present treatment of the PAM, employing the hybridization as perturbation. To study the behavior of the cumulant expansion in the limit $d \to \infty$, it is convenient to consider the direct space GF, given by

$$G^0_\sigma(\mathbf{R_{n,m}}, \omega_\nu) \equiv \frac{1}{N} \sum_{\mathbf{k}} G^0_\sigma(\mathbf{k}, \omega_\nu) \exp[i\mathbf{k}.\mathbf{R_{n,m}}] \quad , \tag{2.8}$$

where $\mathbf{R_{n,m}} = \mathbf{R_n} - \mathbf{R_m}$, as well as its dependence with the minimum number p of n.n. jumps necessary to go from $\mathbf{m}$ to $\mathbf{n}$. When the GF are obtained for large d using the hopping as a perturbation, one immediately shows that $G^0_\sigma(\mathbf{R_{n,m}}, \omega_\nu) \simeq O\,|\theta^p|$,where $\theta = t/\sqrt{2d}$. A similar result is obtained for the "exact" $G^0_\sigma(\mathbf{R_{n,m}}, \omega_\nu)$ of Eq. (2.8), but the discussion will be postponed to a latter section, in which a more general property will be shown.

III. THE HAMILTONIAN OF THE PAM

The Hamiltonian of the whole system is

$$H = H_c + H_f + H_h \quad , \tag{3.1}$$

where H_c is the Hamiltonian of the conduction electrons (c-electrons) discussed in Section II. The second term $H_f = \sum_{j,\sigma} E_\sigma X_{j,\sigma\sigma}$ describes independent localized electrons (f-electrons), where a simple index j has been used to indicate the sites $\mathbf{n}$. The last term is the hybridization Hamiltonian[2], giving the interaction between the c-electrons and the f-electrons:

$$H_h = \sum_{j,\mathbf{k},\sigma} \left(V_{j,\mathbf{k},\sigma}\; X^\dagger_{j,0\sigma}\; C_{\mathbf{k},\sigma} + V^*_{j,\mathbf{k},\sigma}\; C^\dagger_{\mathbf{k},\sigma}\; X_{j,0\sigma} \right) \quad . \tag{3.2}$$

The state space of the f-electrons, at a given site j, is spanned by four states: the vacuum state $\mid j,0\rangle$, the two states$\mid j,\sigma\rangle$ of one f-electron with spin component σ and the state $\mid j,2\rangle$ with two electrons of opposite spin. In the limit of infinite electronic repulsion ($U = \infty$) considered here, the state $\mid j,2\rangle$ is always empty, and can be projected out of the space. The operator $X_{j,0\sigma}$ destroys the electron in state $\mid j,\sigma\rangle$ leaving the site in the vacuum state $\mid j,0\rangle$ with energy $E_{j,0} = 0$, and its Hermitian conjugate $X^\dagger_{j,0\sigma} = X_{j,\sigma 0}$ reverses that process. The Hubbard operators $X_{j,ab}$ are not usually Fermi or Bose operators, and a product rule:

$$X_{j,ab}\; X_{j,cd} = \delta_{bc}\; X_{j,ad} \quad , \tag{3.3}$$

should be employed when the two operators are at the same site. For different sites one should first classify the operators in two families: $X_{j,ab}$ is of the "Fermi type" when $\mid a\rangle$ and $\mid b\rangle$ differ by an odd number of Fermions, and it is of the "Bose type" when they differ by an even number of Fermions. At different sites, two X-operators of the Fermi type anticommute, and they commute when at least one of them is of the Bose type. To complete the definition, the $X_{j,ab}$ should anticommute (commute) with the $C^\dagger_{\mathbf{k},\sigma}$ and $C_{\mathbf{k},\sigma}$ when they are of the Fermi type (Bose type). Sometimes it will be convenient to employ $X(\gamma)$ to describe the Hubbard operators, where $\gamma = (j, \alpha, u)$, and $\alpha = (b, a)$ gives the transition $\mid a\rangle \to \mid b\rangle$ that destroys one electron, i.e. with $\mid b\rangle$ having one electron less than $\mid a\rangle$ as in Ref. 15, and it is often convenient to abbreviate $(\gamma, \tau) = \ell$. The index u is then introduced to describe the inverse transition , so that $X(\gamma) = X_{j,\alpha}$ when $u = -$ and $X(\gamma) = X^\dagger_{j,\alpha}$ when $u = +$, and for the PAM with $U = \infty$ there are only two possible transitions $\alpha = (0, \sigma)$.

The Grand Canonical Ensemble (GCE) of electrons is employed in this problem, and it is useful to introduce

$$\mathcal{H} = H - \mu \left(\sum_{\mathbf{k},\sigma} C^\dagger_{\mathbf{k},\sigma} C_{\mathbf{k},\sigma} + \sum_{j,a} \nu_a\; X_{j,aa} \right) \quad , \tag{3.4}$$

where ν_a is the number of electrons in state $\mid a\rangle$ and μ is the chemical potential. As usual $\mathcal{H}$ is split into

$$\mathcal{H} = \mathcal{H}_0 + H_h \ , \tag{3.5}$$

where H_h will be the perturbation Hamiltonian, and the exact and unperturbed averages of any operator A will be denoted respectively by $< A >_{\mathcal{H}}$ and $< A >$. It is also convenient to denote the exact or Heisenberg "τ evolution" of any operator A with

$$\widehat{A}\,(\tau) = \exp[\mathcal{H}\tau] \ A \ \exp[-\mathcal{H}\tau] \tag{3.6}$$

and employ $A\,(\tau) = \exp[\mathcal{H}_0\tau] \ A \ \exp[-\mathcal{H}_0\tau]$ for the unperturbed case. It is convenient to use the expressions

$$\varepsilon_{j,a} = E_{j,a} - \nu_a\mu \qquad \text{and} \qquad \varepsilon_{\mathbf{k},\sigma} = E_{\mathbf{k},\sigma} - \mu \quad , \tag{3.7}$$

because the energies appear almost always in those combinations.

The c-electron GF employed in the cumulant expansion are:

$$G^o_{c,\sigma}(\mathbf{k},\omega) = -\frac{1}{i\omega - \varepsilon_{\mathbf{k},\sigma}} \quad , \tag{3.8}$$

where the subindex c was added to differentiate them from the unperturbed GF of the f-electron.

$$G^o_{f,\sigma}(\omega) = -\frac{D^0_\sigma}{i\omega - \varepsilon_\sigma} \quad , \tag{3.9}$$

where $D^0_\sigma = \langle X_{\sigma\sigma}\rangle + \langle X_{00}\rangle$.

1. The two Hybridization models

The general hybridization coefficients are given by (cf. Eq. (2.3) in Ref. 2)

$$V_{j,\mathbf{k},\sigma} = \frac{1}{\sqrt{N_s}} V_\sigma(\mathbf{k}) \exp\left(\mathbf{ik.R_j}\right) \qquad . \tag{3.10}$$

The hybridization is purely local when $V_\sigma(\mathbf{k}) = \mathbf{V^0_\sigma}$ is independent of $\mathbf{k}$, because using the Wannier transformation (cf. Eq.(2.2)) in Eq. (3.2) it follows that

$$H_h = \sum_{j,\sigma} \left(V^0_\sigma \ X^\dagger_{j,0\sigma} \ C_{j,\sigma} + (V^0_\sigma)^* \ C^\dagger_{j,\sigma} \ X_{j,0\sigma} \right) \quad . \tag{3.11}$$

The H_h that corresponds to n.n. hybridization is

$$H_h = \sum_{j,\delta,\sigma} \left(V_\sigma \ X^\dagger_{j+\delta,0\sigma} \ C_{j,\sigma} + (V_\sigma)^* \ C^\dagger_{j,\sigma} \ X_{j+\delta,0\sigma} \right) \tag{3.12}$$

where the vectors δ give the position of the d n.n. sites of the origin, and the corresponding $V_\sigma(\mathbf{k})$ is immediately obtained:

$$V_\sigma(\mathbf{k}) = \mathbf{2} \ \mathbf{V}_\sigma \sum_{\alpha=\mathbf{1}}^{\mathbf{d}} \cos(\mathbf{k}_\alpha \ \mathbf{a}) = -\frac{\mathbf{V}_\sigma}{\mathbf{t}} \ \mathbf{E}_{\mathbf{k},\sigma} \quad . \tag{3.13}$$

A. The chain approximation

In figure 1 are shown some of the infinite diagrams that contribute to the exact GF $\left\langle \left(\widehat{X}_{j,\alpha}(\tau)\ \widehat{X}_{j',\alpha'} \right)_+ \right\rangle_{\mathcal{H}}$. The full circles (f-vertices) correspond to the cumulants of the f-electrons and the empty ones (c-vertices) to those of the c-electrons. Each line reaching a vertex is associated to one of the X operators of the cumulant, and the free lines (i.e. those that do not join an empty circle) correspond to the external X operators appearing in the exact GF. An explicit definition of the cumulants can be found in the references[2,3,15],and they can be calculated by employing a generalized Wick's theorem[15–17].

The first diagram in figure 1a corresponds to the simplest free propagator $\left\langle \left(X_{j,\alpha}(\tau)\ X_{j',\alpha'} \right)_+ \right\rangle$, and the second diagram in that figure has an empty circle that corresponds to the conduction electron cumulant, equal to the free propagator $\left\langle \left(C_{k\sigma}(\tau)\ C^{\dagger}_{k\sigma} \right)_+ \right\rangle$. The interaction is represented by the lines (edges) joining two vertices and, because of the structure of the hybridization, they always join a c-vertex to an f-vertex; the number of edges in a diagram gives its order in the perturbation expansion.

Cumulants containing statistically independent operators are zero, and those appearing in the present formalism (with the hybridization as perturbation) vanish unless they contain only X operators at the same site or only C or $C^{\dagger}$ operators with the same k and σ. The only non-zero c-cumulants are of second order, because the uncorrelated c-operators satisfy Wick's theorem. On the other hand, the f-vertices can have many legs, all corresponding to X operators at the same site, like the fourth and sixth order cumulants appearing in the rather more complicated diagram shown in figure 1c.

All the infinite diagrams that contribute to the GF of the f-electron with cumulants of at most second order are shown in figure 1a, and they define the "chain approximation" (CHA) when all the other diagrams are neglected. The corresponding approximation for the GF of the c-electrons corresponds to the diagrams of figure 1b. The diagrams of the CHA usually appear as part of more complicated diagrams, and it is then useful to analyze their behaviour when $d \to \infty$. In the CHA, the GF is given in frequency and $\mathbf{k}$ space by (cf. Eq. (3.10) in Ref.[15])

$$G_{f,\sigma}(\mathbf{k},\omega) = \frac{-(\mathbf{i}\omega - \varepsilon_{\mathbf{k}\sigma})\mathbf{D}^{\mathbf{0}}_{\sigma}}{(\mathbf{i}\omega - \varepsilon_{\sigma})(\mathbf{i}\omega - \varepsilon_{\mathbf{k}\sigma}) - \mid \mathbf{V}(\mathbf{k}) \mid^{\mathbf{2}} \mathbf{D}^{\mathbf{0}}_{\sigma}} \qquad . \tag{3.14}$$

and it would be useful to transform it back to real space to show the dependence with the distance $\mathbf{R}_{i,j}$ between the two sites i and j, as it was done in Eq. (2.8) for the conduction electrons. Because of the lattice translational invariance, it is enough to use the distance $\mathbf{R}_j$ of the site j to the origin, and characterize this site with an $\mathbf{n} = (n_1, \ldots, n_d)$, (cf. Sec. II). The set of indices r with $n_r \neq 0$ will be denoted with $\{r\}_j$, while $s(j)=\sum_1^d n_s$ is the minimum number of n.n. jumps necessary to go from the origin to the site j. In both the local and the n.n. hybridization models, the $G_{f,\sigma}(\mathbf{k},\omega)$ depends on $\mathbf{k}$ only through the $\varepsilon_{\mathbf{k}\sigma} = E_{\mathbf{k}\sigma} - \mu$, and for any given site j one can write

$$E_{\mathbf{k}\sigma} = E_{\sigma}(\{r\}_j, \mathbf{k}) - \theta \sum_{\mathbf{s}\in\{\mathbf{r}\}_{\mathbf{j}}} \cos(\mathbf{a}\ \mathbf{k}_{\mathbf{s}}) \quad , \tag{3.15}$$

where

$$E_{\sigma}(\{r\}_j, \mathbf{k}) = -\theta \sum_{\mathbf{s}\notin\{\mathbf{r}\}_{\mathbf{j}}} \cos(\mathbf{a}\ \mathbf{k}_{\mathbf{s}}) \tag{3.16}$$

and $\theta = t/\sqrt{2d}$. Substituting this relation in Eq. (3.14) one can expand it in a power series of all the $\cos(a\ k_s)$ with $s \in \{r\}_j$ and then transform back to real space to obtain $G_{f,\sigma}(\mathbf{R}_j, \omega)$. Employing the relation

$$\sum_{k_s} \cos^m(k_s\ a)\ \exp(i n_s k_s a) = 0 \quad \text{for} \quad m < n_s \qquad , \tag{3.17}$$

which is a consequence of the cyclic boundary conditions, it follows that

$$G_{f,\sigma}(\mathbf{R}_j,\omega) = O\left|(2d)^{-s(j)/2}\right| \quad . \tag{3.18}$$

The GF for the conduction electrons in the CHA, corresponding to the diagrams in Fig. 1b, is given by:

$$G_{c,\sigma}(\mathbf{k},\omega) = \frac{-(\mathbf{i}\omega - \varepsilon_\sigma)}{(\mathbf{i}\omega - \varepsilon_\sigma)(\mathbf{i}\omega - \varepsilon_{\mathbf{k}\sigma}) - \mid \mathbf{V}(\mathbf{k}) \mid^{\mathbf{2}} \mathbf{D}^{\mathbf{0}}_\sigma} \quad , \tag{3.19}$$

and employing the same derivation used above for the f-electrons it follows that $G_{c,\sigma}(\mathbf{R}_j,\omega) = O\left|(2d)^{-s(j)/2}\right|$. The same relation is obtained in the absence of hybridization, as stated at the end of Section II for $G^0_\sigma(\mathbf{R}_{\mathbf{n},\mathbf{m}},\omega_\nu)$.

To close this section let us emphasize that the present expansion employs H_h as perturbation, and that the exact solution of the conduction problem in the absence of hybridization is included in the zeroth order Hamiltonian. The contribution to the GF joining two sites separated by $s(j)$ n.n. jumps, that is of order $\left|(2d)^{-s(j)/2}\right|$, includes then contributions of any order in the H_c. It is because of this difference that the derivation of Metzner[12] for the Hubbard model had to be modified for the present problem.

All the contributions of H_c would disappear in the case of a band with zero width, but the electronic wave functions would still be extended for the model with n.n. hybridization.

IV. THE CONTRIBUTION OF DIAGRAMS FOR INFINITE DIMENSION

In the present section it will be shown that the only diagrams that remain in the limit $d \to \infty$ are those that are topologically “fully two particle reducible” (f.t.p.r.). These diagrams are defined as those in which any pair of vertices can be separated by cutting one or two edges[18], and are “topologies constructed by linking polygons”[12]. Two points should be made here: the first is that two different polygons (also called loops or rings in what follows) can have at most one vertex in common in the f.t.p.r. topology (see Fig 2a,b). The second point, already stressed by Metzner for the Hubbard model,[12] is that the topology of a diagram can be different from those of its possible embeddings in the lattice, because in the cumulant expansions there is no excluded site restriction in the lattice sums[2], and two different vertices of a diagram can occupy the same site (see Fig. 2c,d). The property stated above refers to the topology of the embeddings, and in the sum of contributions of diagrams that are not f.t.p.r. there may be terms that give non zero contributions because they correspond to a f.t.p.r. topology of the embedding: the diagram in Fig. 2c could contribute when $j = i$, because the topology of its embedding, given by Fig. 2d, is f.t.p.r.

To prove this property it is necessary to modify the derivation given by Metzner for the Hubbard model, for the same reasons given in Section III A for the GF dependence on $s(i)$. The proof of this property is given in the following two subsections, and it can be summarized as follows. Consider first the diagram in Fig. 3a, that corresponds to the sum of loops with all possible lengths. All the embeddings of these diagrams are f.t.p.r., and they give a non-zero contribution to the calculation of the free energy. As a second step, one can consider diagrams like those in Figs. 3c,d, obtained by linking loops of any length at different f-vertices. One could obtain all these diagrams by a procedure similar to the vertex renormalization[2,5,12], with the difference that only insertions of a rather special type are considered. All these diagrams, as well as their embeddings, are f.t.p.r., and a finite contribution of all of them is expected. The next step is to consider diagrams that are not f.t.p.r., like the one shown in Fig 3e, that can be obtained by joining two loops (like that in Fig. 3a) at two different f-vertices. If the family in Fig. 3a gives a finite contribution, one can show that all the contributions to the diagram in Fig. 3e will vanish when the topology of the embedding coincides with that of the diagram, i.e. when the embedding is not f.t.p.r., as it would happen when $i \neq j$. In the special case of $i = j$, (cf. Figs. 2 c,d for a special case of this situation) the embedding is f.t.p.r., and the diagram contribution does not necessarily vanish. Of the two sums over the lattice sites i and j, only one over $i = j$ remains in the limit $d \to \infty$, and this simplifies the calculation of this diagram. In particular, the restriction that in reciprocal space there must be conservation of $\mathbf{k}$ at each vertex is removed[6,14], leaving only a single conservation of $\mathbf{k}$ for all the edges joining the collapsed vertices: this makes the calculation of the diagram much simpler in the limit $d \to \infty$.

A. The f.t.p.r. diagrams

To prove that the contribution of a f.t.p.r. diagram can be finite, let us consider the family of diagrams represented in Fig. 3a. Their contribution does not vanish and can be expressed as

$$\sum_{j_1} \int d\ell_1 \int d\ell_2 \; S_2^0(j_1;\ell_1,\ell_2) \; M_2^0(j_1;\ell_1,\ell_2) \tag{4.1}$$

where

$$M_2^0(j_1;\ell_1,\ell_2) = \left\langle \left(X(\ell_1)X(\ell_2)\right)_+ \right\rangle_c \tag{4.2}$$

is a local cumulant[2] and $\int d\ell_s = \sum_{\alpha_s}\sum_{u_s}\int_0^\beta d\tau_s$. The abbreviations $s \equiv \ell_s$ and $\int ds \equiv \int d\ell_s$ will be used when there is no possibility of confusion. The symbol $S_2^0(j_1;\ell_1,\ell_2) \equiv S_2^0(j_1;1,2)$ corresponds closely to the "self-field"[5] $S_m(j_1;\ell_1,\ell_2,\ldots,\ell_m) \equiv S_m(j_1;1,2,\ldots,m)$, that was employed in Ref. 15 to renormalize vertices, but it gives only "insertions" obtained from simple loops of any length, as represented by the diagrams in Fig 3b; by it definition, all the ℓ_s correspond to the same site, indicated by j_1. The notation $M_2^0(j_1;\ell_1,\ell_2) \equiv M_2^0(j_1;1,2)$ has the same meaning, and reflects the fact that this cumulant is zero unless $j_1 = j_2$ because $X(\ell_1)$ and $X(\ell_2)$ are statistically independent in the unperturbed system when $j_1 \neq j_2$. Note that $S_2^0(j_1;\ell_1,\ell_2)$ depends explicitly on the parameters $j_1;\ell_1,\ell_2$ (where ℓ_i represents $j_i, u_i, \alpha_i = (0,\sigma_i)$ for $i = 1,2$) through the two hybridization constants $V_{j,\mathbf{k},\sigma}$ associated to the edges joining the insertion vertex.

To consider the addition of a simple loop to any f-vertex of a diagram, it is convenient to consider first the simplest possible case, shown in Fig. 3c: its contribution is obtained by substituting the cumulant $M_2^0(j_1;1,2)$ in Eq. 4.1 by

$$\int d3 \int d4 \; M_4^0(j_1;1,2,3,4) \; S_2^0(j_1;3,4) \quad . \tag{4.3}$$

When the loop is added to a site j_1 that is already joined by n edges, the corresponding cumulant $M_m^0(j_1;1,2,\ldots,m)$ suffers a similar substitution. Repeated application of this procedure at all f vertices gives all the possible f.t.p.r diagrams, and as the cumulants are independent of the lattice dimension d and of the site j, this procedure should not affect the order of the contribution with respect to d. The simple loops of Fig. 3a give a finite contribution, so that the contribution of any f.t.p.r diagrams is then of $O\left(|d|^0\right)$.

A similar type of procedure can be applied to the CHA diagrams of the one-particle GF, by successive decoration of the f-vertices with any number of insertions corresponding to the $S_2^0(j_1;\ell_1,\ell_2)$ discussed above. It is then clear that these diagrams will still be f.t.p.r., and that the corresponding GF joining two sites separated by s n.n. jumps will be of order $O\left|(2d)^{-s/2}\right|$, as it was shown in Section III for the CHA.

B. The diagrams that are not f.t.p.r.

To analyze the diagrams that are not f.t.p.r., consider any one of them as a "mother" diagram, and split it into two or more f.t.p.r linked "daughter"diagrams without any edges in common but such that any of them has at least two vertices in common with another daughter diagram, as well as two edges arriving at each of the common vertices. It is clear that any pair of vertices that are common to two daughter diagrams can not be separated in the mother diagram by cutting one or two edges, and one says that they are not "two particle reducible" (t.p.r.).

From all the daughter diagrams choose one as a vacuum diagram and transform the remaining ones into GF by adding external lines of the Bose type (as indicated in Appendix A) to all the vertices that each of them had in common with any other daughter diagram in the mother diagram. Three examples of this procedure are given in Fig 4.

Consider now the real space calculation of the contribution of the daughter diagrams. In Appendix A it is shown that by joining one daughter GF to another diagram and fixing the position of the common vertices, one obtains the order of the contribution of the resulting diagram as the product of those of the building diagrams. In Appendix B it is shown that unless all the external f-vertices of one daughter GF coincide at the same lattice site, the corresponding contribution is of $O\left|(\theta)^p\right|$ with $p \geq 1$, where $\theta = t/\sqrt{2d}$. Taking now the only daughter vacuum diagram and adding successively all the other daughter GF diagrams, the total contribution for given positions of all the GF external vertices will then be $O\left|(\theta)^p\right|$ with $p \geq 1$, unless all the external vertices of each daughter GF coincide at the same lattice site, that can be different for different daughter GF. A typical example of this type of diagram is given in Fig 5b, while in Fig 5c it is shown the corresponding f.t.p.r. topology of the embedding when the vertices that are not t.p.r. in the diagram are at the same lattice site.

It is then clear that in the sum over the vertices that are common to all the daughter diagrams, each of the terms will be at best of $O\left|\theta\right|$, and would vanish in the limit $d \to \infty$, unless all the external vertices of each daughter diagram are at the same lattice site, that can be different for different daughter diagrams. One can conclude that the contribution of the mother diagram would vanish when any pair of vertices i and j that are not t.p.r. occupy different lattice sites, because in that case, it is always possible to separate from the mother diagram a daughter GF that has i and j in common with the rest of the diagram. In that case, only a sum over $i = j$ should remain from the unrestricted sum over i and j, and those two vertices then become t.p.r. in the embedding of the diagram (this is illustrated in Figs. 5b,c). This reduction of the terms that contribute to the lattice summations has been already described, and called "collapse of vertices", in the study of the U-perturbation theory in high dimensions[14,18]: this property will also be given the same name in the present work.

One important point to notice, is that the collapse of vertices occurs only in the embedding of the diagram, and that the rules for calculating the contribution should be applied to the original diagram (i.e. it would be the diagram of Fig. 5b in the examples given) and not to the collapsed diagram of the embedding (i.e. the diagram in Fig. 5c).

As in the collapse of i and j the two independent lattice summations over the vertices i and j are replaced by a single lattice summation over $i = j$, it is easy to see from the derivation of the contribution rules in reciprocal space (cf. Section III D in Ref. 2) that the two independent momentum conservation at each of the two collapsed vertices becomes a single conservation of the wave vectors corresponding to all the internal edges joining them. When all the pair of vertices that are not t.p.r. have been collapsed, one can see that at every vertex of the embedding of a vacuum or one particle GF diagram, all the edges can be arranged in pairs with momentum $\mathbf{k_s}$ and -$\mathbf{k_s}$ respectively (cf. Fig. 5c as a typical example) It then follows that the momentum conservation at the collapsed vertices are automatically satisfied, and most of the usual restrains on the momentum integration disappear in the limit $d \to \infty$.

V. SUMMARY AND CONCLUSIONS

The cumulant expansion of the PAM[2] was considered in the limit of infinite spatial dimensions ($d \to \infty$) for two types of hybridization models: the purely "local" hybridization and the "nearest neighbor" (n.n.) one. As the systems usually described by the PAM have a bandwidth much larger than the hybridization energies, the unperturbed Hamiltonian is chosen to include the exact solution of the conduction band electrons in the absence of hybridization. It was then necessary to modify the derivation employed by Metzner[12] for the cumulant expansion of the Hubbard model, in which the hopping Hamiltonian is used as perturbation. The basic result presented here is that in spite of this change the PAM shows, for the two hybridization models considered, the same type of simplifications that occur in the diagrammatic cumulant expansion of the Hubbard model when $d \to \infty$.

Only the linked diagrams contribute to the general cumulant expansion, and there is a vertex collapse when $d \to \infty$ for those diagrams that are not f.t.p.r. A diagram is not f.t.p.r. when at least two vertices i and j can not be separated by cutting only one or two edges of the diagram, and their collapse means that from the two independent summations over i and j that are necessary to calculate their contribution, only a summation over $i = j$ remains. The topology of the embedding is different from that of the diagram itself when $i = j$, and the collapse is repeated until the topology of the embedding becomes f.t.p.r. One important point to notice is that, after the collapse of vertices, the rules for calculating the contribution should be applied to the original diagram and not to the collapsed diagram of the embedding.

When the two independent summations over i and j of the diagram become a single summation over $i = j$ because the two vertices i and j collapse, the two separate conservations of $\mathbf{k}$ at these vertices become a single conservation of the $\mathbf{k}$ corresponding to all the edges joining both i and j. As a consequence, most of the usual restrains on the momentum integration disappear in the limit $d \to \infty$, and the calculation of many diagrams is very much simplified by this change. One should note that the vertex collapse does not alter the calculation over frequencies, which keep their conservation at all the diagram vertices, even when $d \to \infty$.

Employing the cumulant expansion, Metzner has shown[12] that the single-particle properties of the Hubbard model in the limit $d \to \infty$, can be described as that of independent electrons "hopping between dressed atoms characterized by an effective Green's function". A similar derivation can be employed for the PAM, and the exact one electron GF is given by the family of diagrams in Fig. 1a, but using an effective cumulant $M_{2,\sigma}^{eff}(\omega)$ for the f-electron vertices instead of the bare one $M_{2,\sigma}^{0}(\omega)$. The effective cumulant $M_{2,\sigma}^{eff}(\omega)$ is given by the contribution of all the diagrams of $G_\sigma(\mathbf{R_{n,m}} = 0, \omega)$ that can not be separated by cutting a single edge (usually called "irreducible diagrams"), where $G_\sigma(\mathbf{R_{n,m}} = 0, \omega)$ is the exact GF of the f-electrons in the real space representation for $\mathbf{n} = \mathbf{m}$. This property is only valid in the limit $d \to \infty$, so that all the diagrams that are not f.t.p.r have their vertices collapsed until the associated embeddings are f.t.p.r. The exact GF can then be written

$$G_{f,\sigma}(\mathbf{k},\omega) = M_{2,\sigma}^{eff}(\omega)\ \frac{1}{1- \mid V(k) \mid^2 G_{c,\sigma}^{o}(k,\omega)\ M_{2,\sigma}^{eff}(\omega)} \tag{5.1}$$

A practical difficulty in the study of correlated electron systems with cumulant expansions, is that the higher order cumulants rapidly become very laborious to calculate. To consider in some way the higher order cumulants, we are studying the substitution of $M_{2,\sigma}^{eff}(\omega)$ by an approximate quantity $M_{2,\sigma}^{at}(\omega)$, derived from an exactly soluble model. To this purpose we use the same Anderson periodic model but in the atomic limit[19], i.e. when the hopping of the conduction electrons is eliminated by taking a conduction band of zeroth width. This attempt will be discussed in another publication, and the present work provides an essential guidance to that study, by showing that all the cumulant diagrams present in $M_{2,\sigma}^{eff}(\omega)$ are also present in the approximate $M_{2,\sigma}^{at}(\omega)$. Although the hopping is missing from the $M_{2,\sigma}^{at}(\omega)$, the exact solution of the conduction band shall appear in the "hopping between dressed atoms"[12] through the $G_{c,\sigma}^{o}(k,\omega)$ in Eq. (5.1).

ACKNOWLEDGMENTS

The authors would like to thank Prof. Roberto Luzzi for critical comments, and to acknowledge financial support from the following agencies: CAPES-PICD (MSF), FAPESP and CNPq (MEF). This work was done (in part) in the frame of the Associate Membership Programme of the International Centre for Theoretical Physics, Trieste ITALY (MEF).

APPENDIX A: SEPARATION OF VERTICES

In Section IV it is shown that the contribution of a "mother" vacuum diagram that is not f.t.p.r. can be estimated from those of several f.t.p.r. "daughter" diagram that are derived from the original one. The daughter diagrams are obtained by separating the mother diagram into several f.t.p.r. subdiagrams: a vacuum diagram plus several GF diagrams obtained by adding external lines of the Bose type to the vertices that these separated diagrams have in common in the mother diagram. To show the procedure, it is convenient to analyze a simple case, like that of Fig. 5a, and consider only a single vertex in real space, as shown in Fig 6a, assuming first that it does not belong to the vacuum daughter diagram. Writing only that part P of the total contribution to the mother diagram that have parameters connected to the particular vertex under consideration, one obtains

$$P = \sum_j \int d1 \int d2 \int d3 \int d4 \sum_{\mathbf{k_1 k_2}} \sum_{\mathbf{k_3 k_4}} \exp\left[-i\left(\mathbf{k_1} - \mathbf{k_2} + \mathbf{k_3} - \mathbf{k_4}\right).\mathbf{R}_j\right]$$
$$\times V(1)V^*(2)V(3)V^*(4)G_c^0(1)G_c^0(2)G_c^0(3)G_c^0(4)M_4^0(j,1,2,3,4) \tag{A1}$$

where the $G_c^0(s)$ are the c-electron GF, and the other abbreviations are those introduced in Section IV. The time or frequency dependence has been left out because it only plays a trivial role in this proof. The corresponding contribution P_a to one daughter diagram for fixed values ℓ_1, ℓ_2 of the internal lines joining the vertex, and with an added external line of momentum K_a and parameters ℓ_a is

$$P_a(\mathbf{K}_a, \ell_a, \ell_1, \ell_2) = \frac{1}{\sqrt{N}} \sum_{\mathbf{k_1 k_2}} \sum_j \exp\left[-i\left(\mathbf{k_1} - \mathbf{k_2} + \mathbf{K_a}\right).\mathbf{R}_j\right] \times M_3^0(j,a,1,2)\; V(1)V^*(2)G_c^0(1)G_c^0(2) \quad , \tag{A2}$$

and the contribution $P_b(\mathbf{K}_b, \ell_b, \ell_3, \ell_4)$ of the other daughter diagram is trivially obtained by replacing $a, 1, 2$ by $b, 3, 4$.

Transforming $P_a(\mathbf{K}_a, \ell_a, \ell_1, \ell_2)$ to real space, the contribution associated to a site $\mathbf{R}_j$ is given by

$$\begin{aligned} P_a(\mathbf{R}_j, \ell_a, \ell_1, \ell_2) &= \frac{1}{\sqrt{N}} \sum_{\mathbf{K}_a} \exp\left(i\mathbf{K}_a.\mathbf{R}_j\right) P_a(\mathbf{K}_a, \ell_a) \\ &= \sum_{\mathbf{k_1 k_2}} \exp\left[-i\left(\mathbf{k_1} - \mathbf{k_2}\right).\mathbf{R}_j\right] V(1)V^*(2)G_c^0(1)G_c^0(2)M_3^0(j,a,1,2) \end{aligned} \tag{A3}$$

and a similar expression $P_b(\mathbf{R}_j, \ell_b)$ is obtained for the other daughter diagram. It is clear that the only difference between the product $P_a(\mathbf{R}_j, \ell_a, \ell_1, \ell_2)\; P_b(\mathbf{R}_j, \ell_b, \ell_3, \ell_4)$ and the term corresponding to $\vec{R}_j$ and fixed $\ell_1, \ell_2, \ell_3, \ell_4$ in Eq. A1 is given by the cumulants M^0, which are all independent of both $\mathbf{R}_j$ and of the space dimension d. It then follows that

$$P = \int d1 \int d2 \int d3 \int d4\; \frac{M_4^0(j,1,2,3,4)}{M_3^0(j,a,1,2)M_3^0(j,b,3,4)} \times \sum_j P_a(\mathbf{R}_j, \ell_a, \ell_1, \ell_2)\; P_b(\mathbf{R}_j, \ell_b, \ell_3, \ell_4) \tag{A4}$$

gives the dependence of P with d.

When one of the two daughter diagrams is the chosen as the vacuum one, it is necessary to consider the corresponding contribution

$$\overline{P}(\mathbf{R}_j, \ell_1, \ell_2) = \sum_{\mathbf{k_1 k_2}} \exp\left[-i\left(\mathbf{k_1} - \mathbf{k_2}\right).\mathbf{R}_j\right] V(1)V^*(2)G_c^0(1)G_c^0(2)M_2^0(j,1,2) \quad , \tag{A5}$$

that was obtained replacing $M_3^0(j,a,1,2)$ by $M_2^0(j,1,2)$ in Eq. (A3): this is the quantity that appears in the corresponding vertex of the vacuum daughter diagram. In this case, instead of Eq. (A4) one has the relation

$$P = \int d1 \int d2 \int d3 \int d4 \frac{M_4^0(j,1,2,3,4)}{M_2^0(j,1,2)M_3^0(j,b,3,4)} \times \sum_j \overline{P}(\mathbf{R}_j, \ell_1, \ell_2)\; P_b(\mathbf{R}_j, \ell_b, \ell_3, \ell_4) \quad . \tag{A6}$$

This are the relations employed in Section IV to prove that only embeddings that are f.t.p.r. give a non zero contribution, thus leading to the collapse of vertices when they can not be separated by cutting at most two edges.

APPENDIX B: DIAGRAMS THAT ARE NOT F.T.P.R.

In the procedure discussed in Section IV a "mother" vacuum diagram that is not f.t.p.r. is separated into several subdiagrams that have that property. As discussed before, one of the daughter diagrams is chosen as a vacuum diagram, and the remaining ones are GF diagrams obtained by adding external lines of the Bose type to the vertices that these GF diagrams share with other daughter diagrams in the mother diagram. Let us consider one of the GF daughter diagrams in the reciprocal space, with momenta $\mathbf{K}_\upsilon$, indices u_υ and transitions α_υ ($\upsilon = 1, 2, \ldots, n$) assigned to the $n \geq 2$ external vertices, where the α_υ correspond to pair of states with equal number of electrons, i.e. to operators X_α of the Bose type. All these external parameters will be indicated by $\{\mathbf{K}_\upsilon, \ell_\upsilon\}$, while $\{\ell\}_{int}$ will be used for the set of ℓ associated to the internal edges joining all the external vertices. The contribution corresponding to fixed $\{\ell\}_{int}$ of a split diagram is denoted by $F\left(\{\mathbf{K}_\upsilon, \ell_\upsilon\}, \{\ell\}_{int}\right)/N^{n/2}$, where the factor $1/\sqrt{N}$, associated to each external line joining an f-vertex (cf. Rule 3.7 f in Ref. 2), has been explicitly written. To transform from $\mathbf{K}_\upsilon$ to position variables $\mathbf{R}_\upsilon$ one should calculate

$$\overline{F}\left(\{\mathbf{R}_\upsilon\}, \{\ell\}\right) = \left(\sqrt{N}\right)^{-n} \sum_{\{\mathbf{K}_\upsilon\}} \left(F\left(\{\mathbf{K}_\upsilon, \ell_\upsilon\}, \{\ell\}_{int}\right)/N^{n/2}\right) \exp\left[i \sum_{\upsilon=1}^{n} \mathbf{K}_\upsilon . \mathbf{R}_\upsilon\right] \tag{B1}$$

where $\{\ell\}$ denotes all the ℓ, both internal and external. From the translational invariance of the system (or from wave vector conservation at all the vertices) it follows that $\sum_\upsilon \mathbf{K}_\upsilon = 0$, so that

$$\overline{F}\left(\{\mathbf{R}_\upsilon\}, \{\ell\}\right) = \left\{ \prod_{\upsilon=1}^{n-1} \left(\frac{1}{N} \sum_{\mathbf{K}_\upsilon} \exp\left[i\mathbf{K}_\upsilon . \left(\mathbf{R}_\upsilon - \mathbf{R}_n\right)\right] \right) \right\} \ F\left(\{\mathbf{K}_\upsilon, \ell_\upsilon\}, \{\ell\}_{int}\right) \tag{B2}$$

In the two hybridization models considered in this work, the external wave vectors $\mathbf{K}_\upsilon$ appear in $F\left(\{\mathbf{K}_\upsilon, \ell_\upsilon\}, \{\ell\}_{int}\right)$ only through the delta that gives the wave vector conservation at each external vertex. The internal wave vectors $\mathbf{k}$ appear through the $E_{\mathbf{k},\sigma}$ in $G^o_{c,\mathbf{k},\sigma}(\omega)$ (i.e. the c-electron GF of Eq.(3.8)) and also in the $V_\sigma(\mathbf{k}) = -\left(\mathbf{V}_\sigma/\mathbf{t}\right)\ \mathbf{E}_{\mathbf{k},\sigma}$ (cf. Eq. (3.10)) for the n.n. hybridization model. When the wave vector conservation at all vertices is considered explicitly, the number of summations over internal $\mathbf{k}$ is reduced, but the arguments of the $E_{\mathbf{k},\sigma}$ become linear combinations of both the remaining external and internal $\mathbf{k}$. To illustrate this result, consider the diagram in Fig. 7: applying momentum conservation one can write

$$\begin{aligned} &F\left(\{\mathbf{K}_a, \ell_b, \mathbf{K}_a, \ell_a\}, \{\ell_1, \ell_2, \ell_3, \ell_4\}\right) = \\ &\sum_{\mathbf{k_1}} M_3^0(b,1,2)\ M_3^0(a,3,4)\, \left|V_\sigma(\mathbf{k_1})\right|^2 \left|V_\sigma(\mathbf{k_1} - \mathbf{K_a})\right|^2 G^o_{c,\sigma_1}(\mathbf{k_1})\ \mathbf{G^o_{c,\sigma_2}}(\mathbf{k_1} - \mathbf{K_a}), \end{aligned} \tag{B3}$$

where the frequencies are not explicitly written because they don't play any role in this analysis. There is only a single summation over $\mathbf{k_1}$, because from the sum over $\mathbf{k_2}$ only $\mathbf{k_2} = \mathbf{k_1} - \mathbf{K_a}$ remains.

To study the general case, it is convenient to write (cf. Eq. (2.4))

$$E_{\mathbf{k},\sigma} \equiv E_\sigma(\mathbf{k}) = -\sum_{\mathbf{s=1}}^{\mathbf{d}} \theta_{\mathbf{s}} \cos\left(\mathbf{a}\ \mathbf{k_s}\right) \tag{B4}$$

so that $F\left(\{\mathbf{K}_\upsilon, \ell_\upsilon\}, \{\ell\}_{int}\right)$ can be expanded in series of the θ_s, putting $\theta_s = \theta = t/\sqrt{2d}$ at the end of the derivation. To analyze the dependence of $\overline{F}\left(\{\mathbf{R}_\upsilon\}, \{\ell\}\right)$ with θ, it is convenient to concentrate first on a given external vertex υ, and write $\mathbf{K}_\upsilon = \mathbf{Q} = (Q_1, \ldots, Q_d)$ and $\mathbf{R}_\upsilon - \mathbf{R}_n = \mathbf{R} = (R_1, \ldots, R_d)$. The Eq. (B2) shows that for the given external vertex υ, there is a $\sum_{Q_s} \exp\left(i\ Q_s R_s\right)$ applied to $F\left(\{\mathbf{K}_\upsilon, \ell_\upsilon\}, \{\ell\}_{int}\right)$ for each dimension $s = 1, \ldots, d$ of the space, and when for a given s it is $R_s \neq 0$, all the terms independent of θ_s in the expansion of $F\left(\{\mathbf{K}_\upsilon, \ell_\upsilon\}, \{\ell\}_{int}\right)$ will cancel out (cf. Eq. (3.17)). It then follows that $\overline{F}\left(\{\mathbf{R}_\upsilon\}, \{\ell\}\right) = O\left|\theta^p\right|$, where $p \geq p^0$ and p^0 is the number of dimensions for which there are non zero components s for at least one of the $n-1$ vectors $\mathbf{R}_\upsilon - \mathbf{R}_n$. One can then conclude that unless all the R_υ coincide, the $\overline{F}\left(\{\mathbf{R}_\upsilon\}, \{\ell\}\right)$is at least of $O\left|\theta\right|$ and it vanishes when $d \to \infty$. This property was used to prove the collapse of vertices discussed in Section IV for diagrams that are not f.t.p.r.

[1] Hewson A C 1993 *The Kondo problem to Heavy Fermions (*Cambridge U.P. Cambridge)
Schlottmann P 1989 *Phys. Rep.* **181** 1
Fulde P 1988 *Solid State Physics* **41** 1

[2] Figueira M S, Foglio M E and Martinez G G 1994 *Phys. Rev.* B **50** 17933

[3] Hubbard J 1966 *Proc. R. Soc. London, Ser.* A **296** 82

[4] Hubbard J 1964 *Proc. R. Soc. London, Ser.* A **276** 238; Hubbard J 1964 *Proc. R. Soc. London, Ser.* A **277** 237 Hubbard J 1964 *Proc. R. Soc. London, Ser.* A **281** 401 (these are the first three papers of a series of six)

[5] Wortis M 1974 in *Phase Transitions and Critical Phenomena*, edited by C. Domb and M. S. Green (Academic,London), Vol. **3**, pg.113

[6] Metzner W and Vollhardt D 1989 *Phys. Rev. Lett.* **62** 324

[7] Georges A, Kotliar G, Krauth W and Rozenberg M J 1996 *Rev. Mod. Phys.* **68** 13

[8] Jarrel M, Akhlaghpour H and Pruschke Th 1993 *Phys. Rev. Lett.* **70** 1670
Jarrel M 1995 *Phys. Rev.* B **51** 7429

[9] Mutou T and Hirashima D S 1994 *J. Phys. Soc. (Jpn.)*, **63** 4475
Mutou T and Hirashima D S 1995 *J. Phys. Soc. (Jpn.)*, **64** 4799

[10] Mutou T and Hirashima D S 1996 *J. Phys. Soc. (Jpn.)*, **65** 369

[11] Saso T and Itoh M 1996 *Phys. Rev.* B **53** 6877

[12] Metzner W 1991 *Phys. Rev.* B **43** 8549

[13] Tsung-han Lin and Falicov L M 1980 *Phys. Rev.* B **22** 857

[14] Muller Hartmann E 1989 *Z. Phys.* B **74** 507

[15] Figueira M S and Foglio M E 1996 *J. Phys.: Condens. Matter* **8** 5017

[16] A. C. Hewson 1977 *J. Phys. C: Solid State Phys.* **10** 4973

[17] Yang D H Y and Wang Y L 1975 *Phys. Rev.* B **10** 4714

[18] Metzner W and Vollhardt D 1990 *Helv. Physica Acta* **63** 364

[19] Foglio M E and Falicov L M 1979 *Phys. Rev.* B **20** 4554

FIG. 1. Typical cumulant diagrams for one-particle GF (a) The diagrams of the chain approximation (CHA) for the f-electron, represented by the filled square to the right, (b) As (a) but for the c-electrons , represented by an empty square. (c) A more complicated diagram, with cumulants of fourth and sixth order.

FIG. 2. Examples of relevant topologies in the limit $d \to \infty$. a)Fully two particle reducible (f.t.p.r.): any pair of vertices can be separated by cuting two edges. Note that all pairs of loops have at most one vertex in common. b) The diagram is not f.t.p.r. c) The topology of the diagram and that of the embedding are the same when $i \neq j$. d) The embedding topology that corresponds to the diagram in c) when $i = j$.

FIG. 3. a) The sum of all the simple loops of any length. b) Diagrams of an insertion with contribution $S_2^0(j_1;\ell_1,\ell_2)$, obtained by fixing the site j_1 and the parameters ℓ_1,ℓ_2 of one conduction vertex (that is considered external) of the diagrams in a). The full circle in these vertices, corresponding to the cumulant $M_2^0(j_1;\ell_1,\ell_2)$, is removed from the diagrams and is replaced by 1 in $S_2^0(j_1;\ell_1,\ell_2)$. c) A f.t.p.r diagram obtained by joining two simple loops at an f-vertex. d) Family of four linked loops that give a f.t.p.r diagram. e) Family of diagrams obtained by linking two loops at two different f-vertices: it is not f.t.p.r.

FIG. 4. Three examples of separation of a mother vacuum diagram into several daughter diagrams. a) Simplest case of separation with two common vertices. b),c) Separation in three daughter diagrams with a total of four shared vertices.

FIG. 5. a) A family of f.t.p.r diagrams that give a finite contribution for large d. b)Family of diagrams obtained by joining pairs of f.t.p.r diagrams in two common vertices; the diagrams are not f.t.p.r. c) The f.t.p.r topology of the embedding of b) when $i = j$. Note that the diagram contribution is calculated with the diagram b) and not with c), but replacing the two independent summations over i and j by a single one over $i = j$.

FIG. 6. Separation of a vertex with four edges into a pair of vertices with two edges each.

FIG. 7. A simple f.t.p.r diagram. The conservation of moment $\mathbf{k}$ at the vertex b gives $\mathbf{k_1} - \mathbf{k_2} - \mathbf{K_b} = \mathbf{0}$ for $u_b = -1$ and that at vertex a gives $\mathbf{k_2} - \mathbf{k_1} + \mathbf{K_a} = \mathbf{0}$ for $u_a = +1$, so that $\mathbf{K}_a = \mathbf{K}_b$ as should be expected from the translational invariance of the system. Only one summation over $\mathbf{k_1}$ remains because $\mathbf{k_2} = \mathbf{k_1} - \mathbf{K_a}$.

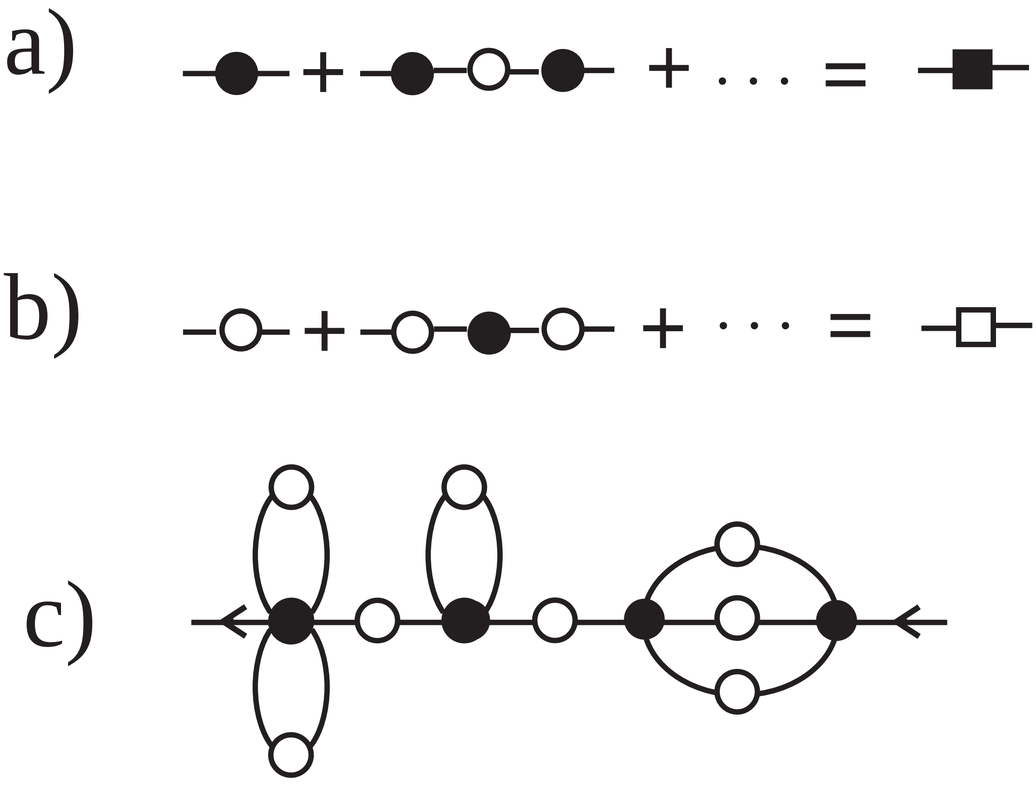
a)
+
+ . . .
=
b)
+
+ . . .
=
c)

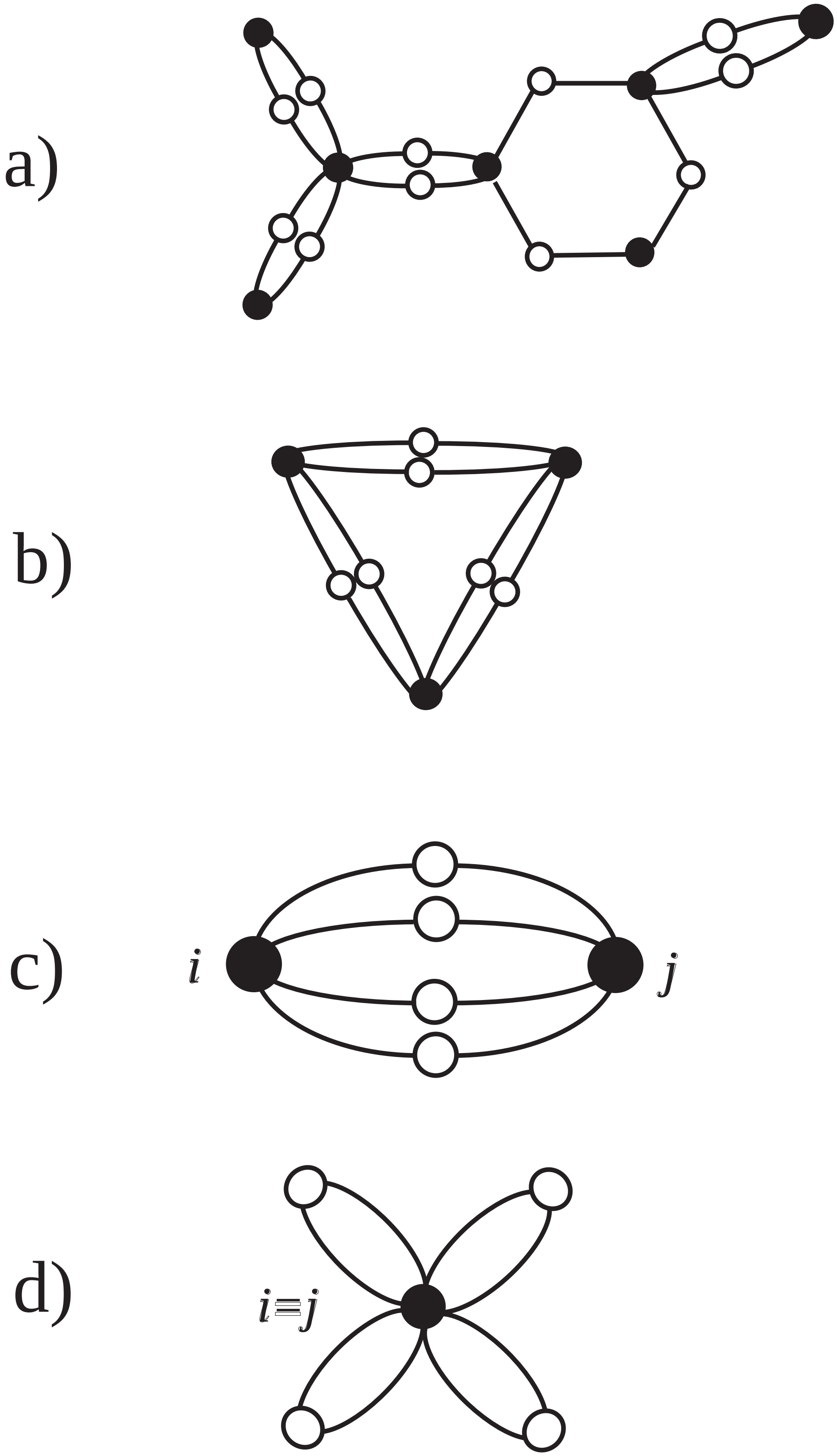
a)
b)
c)
i
j
d)
i=j

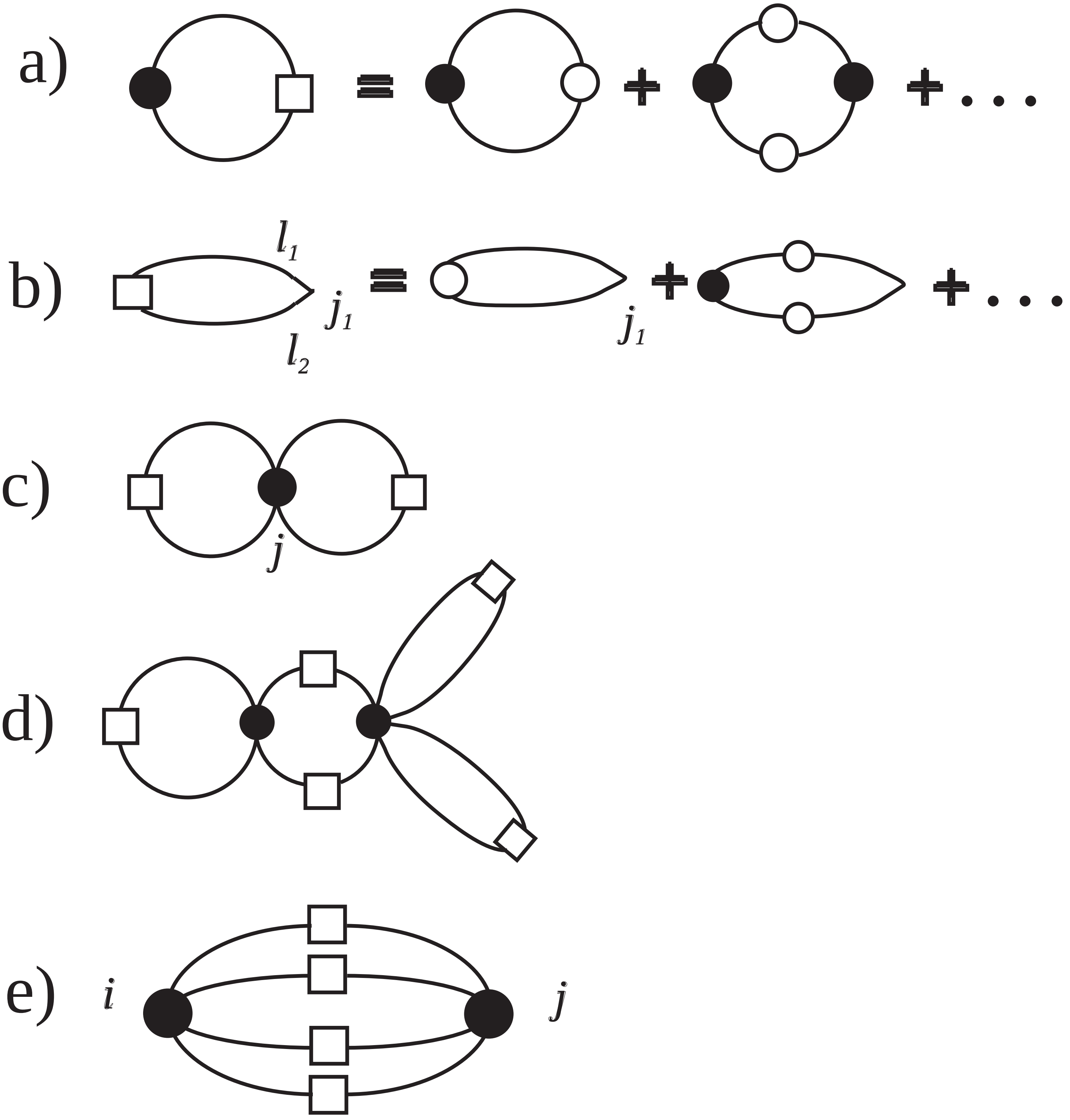
a)
b)
l_1
j_1
l_2
j_1
c)
j
d)
e)
i
j

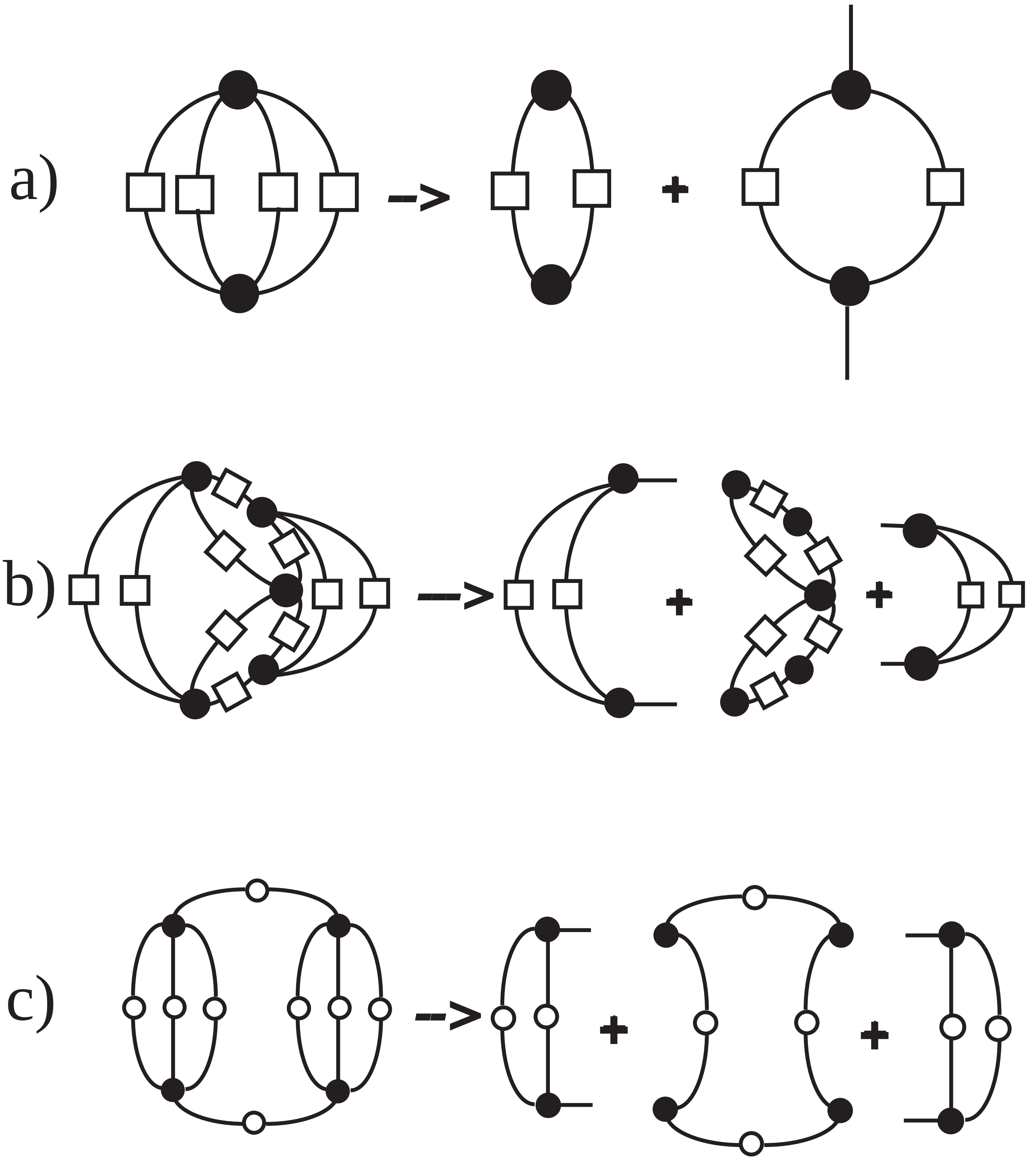
a)
-->
+
b)
-->
+
+
c)
-->
+
+

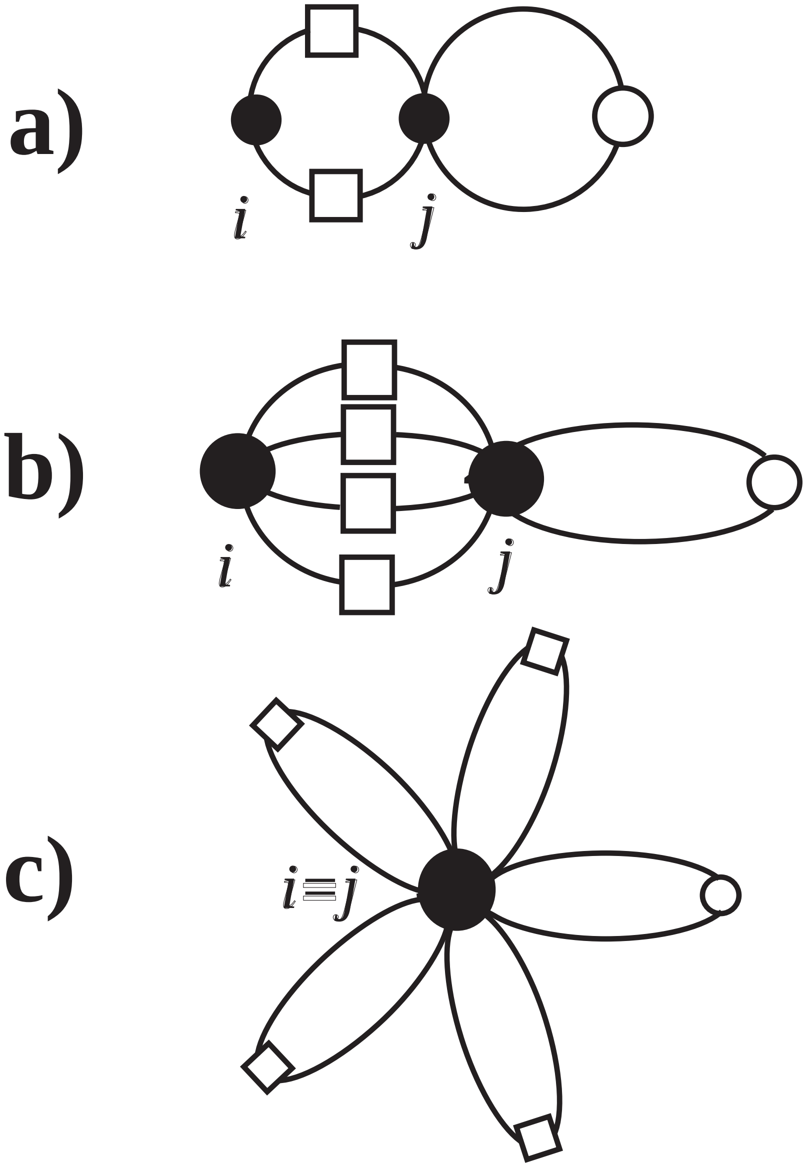
a)
i
j
b)
i
j
c)
i≡j

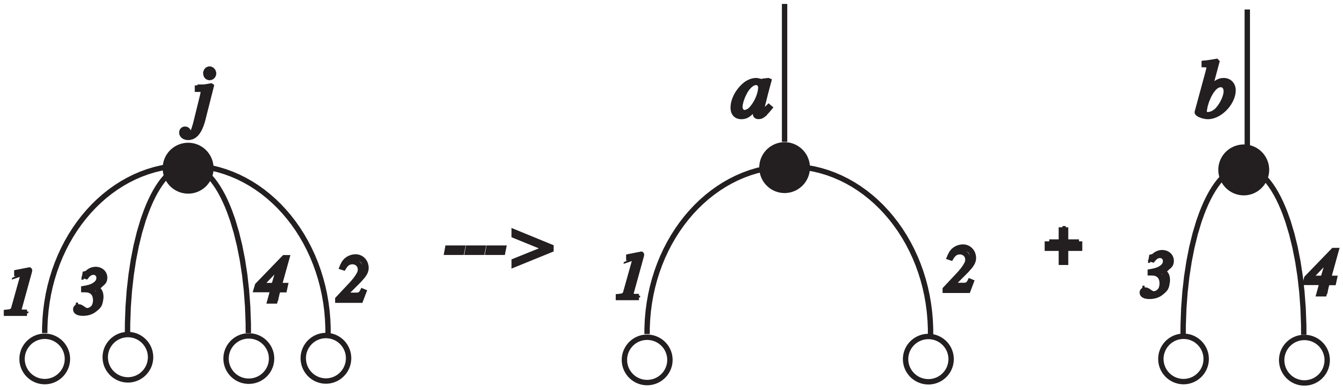
j
-->
a
+
b

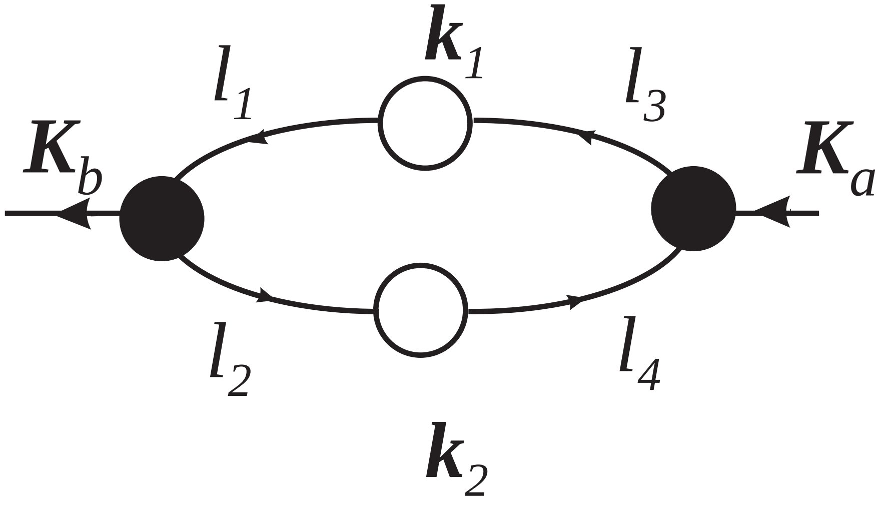

$\boldsymbol{k}_1$
l_1
l_3
$\boldsymbol{K}_b$
$\boldsymbol{K}_a$
l_2
l_4
$\boldsymbol{k}_2$